ACS APPLIED MATERIALS & INTERFACES

LETTER

www.acsami.org

Simple Fabrication of a Pd−P Film on a Polymer Membrane and Its Catalytic Applications

Jeong Hoon Byeon[†] and Young-Woo Kim[*,‡]

[†]Department of Chemistry, Purdue University, Indiana 47907, United States

[‡]Department of Automotive Engineering, Hoseo University, Asan 336-795, Republic of Korea

ABSTRACT:

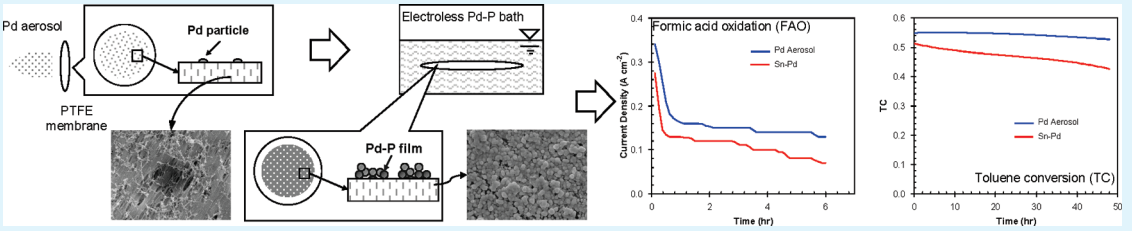

Composites were prepared by a surface activation by aerosol deposition of Pd nanoparticles (Pd nano seeds) on a poly(tetrafluoroethylene) membrane and subsequent Pd−P film formation by electroless deposition. Activation of the membrane processed by an ambient Pd spark discharge and subsequent fixation of the spark produced Pd nano seeds. Characterizations for electroless Pd−P films indicated that P entered into the crystal lattice of Pd and formed an alloy. The fabricated composites were applied to catalytic applications of formic acid oxidation (FAO) and toluene conversion (TC). The composite catalysts from the simple activation had more stable performances of FAO and TC than those from the conventional Sn−Pd activation, and their better performances might have originated from better purity due to the simple activation that only introduced pure Pd nano seeds.

KEYWORDS: composite catalyst, Pd nano seed, Pd−P film, electroless deposition, simple activation, catalytic applications

INTRODUCTION

Proton-exchange membrane fuel cells (PEMFCs) and direct methanol fuel cells (DMFCs) are attracting more and more attention as environmentally friendly power sources for transportation and stationary applications. Recently, the advantages of direct formic acid fuel cells (DFAFCs) have been progressively recognized compared to DMFCs.[1] Pd catalysts are of interest as anodic catalysts for DFAFCs, and it is known that Pd possesses good electrocatalytic activity for the oxidation of formic acid.[2] However, the Pd catalyst has some drawbacks. In particular, Pd is easily oxidized compared with Pt. Thus, one of the disadvantages of Pd as an anodic catalyst is its instability.[3] In order to improve the stability of the Pd catalyst, Pd-based composite catalysts are investigated. Most of the reported composite catalysts are composed of Pd and other metallic elements, such as Pt and Au.[4,5] More recently, the introduction of a nonmetal element, such as P, into the Pd catalyst is a promising strategy to develop alternative materials as catalytic electrodes.[6] Moreover, a composite catalyst incorporating P is also considered a suitable catalyst for the conversion of harmful volatile organic compounds (VOCs). The catalyst demonstrates advantages compared to either Pt or Pd only, such as in its stability and low cost and even higher activity depending on the organic compound.[7]

For fabricating metallic catalysts, electroless deposition (ELD) has strong advantages over sputtering, chemical vapor deposition, and electrodeposition, particularly with respect to its cost performance, use of nonconductive substrates with complex shapes, and simple equipment.[8,9] On the other hand, the initiation of the ELD process is preceded by surface activation to provide ELD initiation sites (i.e., seeds or initiators) on the substrate's surface. The seed is an electron carrier in the transfer of electrons from the reducer to metal ions in an ELD bath.[10] Concerning conventional Sn-based wet activation,[11,12] it is suggested that the introduction of Sn leads to the gradual degradation of the catalyst performance due to undesirable alloying.[13] Aerosol activation involves fewer steps than the Sn-based conventional activation and does not introduce unwanted impurities.[14]

In this paper, the authors present the result of using the Pd−P film on a polymer membrane [poly(tetrafluoroethylene), PTFE] as a Pd-based composite catalyst, fabricated by an ELD using Pd nano seeds produced by an ambient spark discharge to apply to a formic acid oxidation (FAO) and a toluene conversion (TC). The incorporation of metallic films into polymer matrixes is an area of interest for the study of interactions between the films and polymers.[13] In particular, there has been increasing interest in the preparation of Pd-based films on a polymer support because of their much improved catalytic activity. However, the use of Pd−P composite catalysts is still limited to only a few studies,[15,16] and therefore there is not much information available concerning the appropriate fabrication process.[17]

Received: May 17, 2011
Accepted: July 7, 2011
Published: July 07, 2011

dx.doi.org/10.1021/am200613w | *ACS Appl. Mater. Interfaces* 2011, 3, 2912–2918

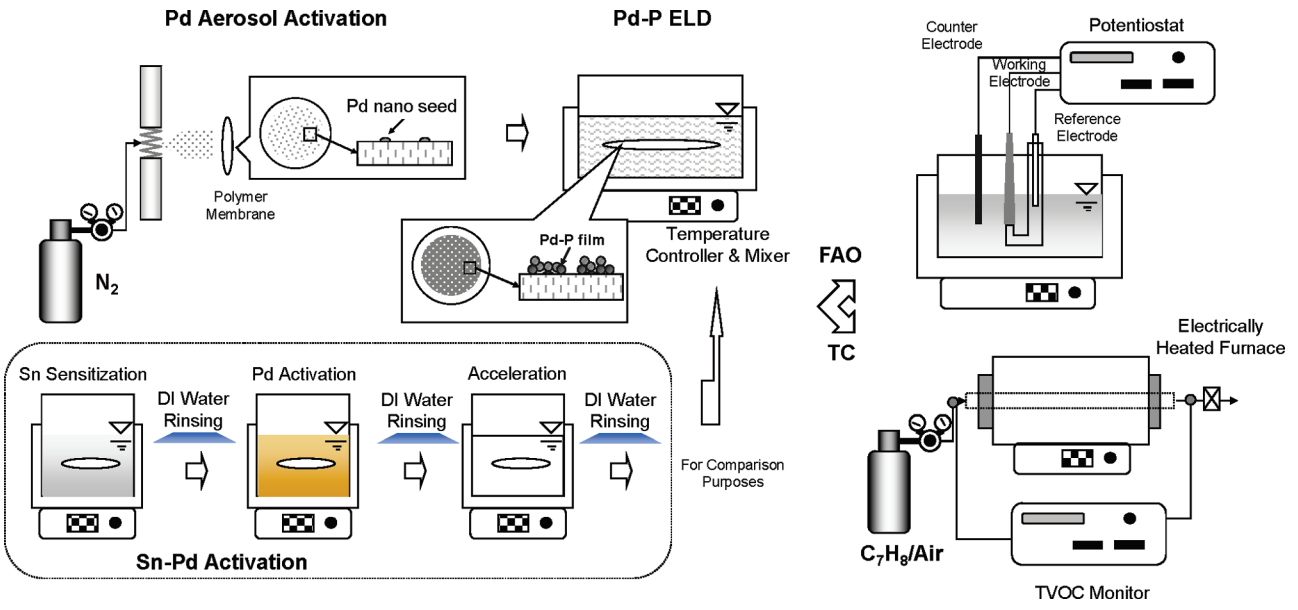

Figure 1. Diagram of the fabrication procedures and catalytic applications.

EXPERIMENT

Figure 1 shows a diagram of the method used to fabricate Pd−P composite catalysts. A spark discharge was used to produce Pd nano seeds under ambient conditions as seeds (or initiators) for an ELD,[14] and the seeds were captured by the polymer membrane (0.2 μm pore size, 47 mm diameter; 11807-47-N, Sartorius) by a physical filtration (i.e., mechanical filtration, mainly by diffusion, of Pd nanoparticles on surfaces of the membrane) under 4.65 cm s^{-1} of gas face velocity. Indeed, primary Pd nano seeds were produced by the spark discharge at atmospheric pressure in controlled conditions (the flow rate of nitrogen gas as well as the spark frequency and energy) to prevent agglomeration, which was critical for the deposition of individual primary Pd nano seeds and related catalytic activity.[18−21] The polymer (PTFE) was selected because of its superior chemical resistance (hydrophobicity), good thermal stability, and high mechanical strength.[22] Furthermore, the hydrophobicity of the support favored the adsorption of organic compounds over the catalyst surface.[23] After annealing at 240 °C, the seeds' fixed, so-called "activated", membrane was immersed horizontally in an ELD bath to form a Pd−P film on the surface of the membrane. The primary Pd nano seeds were eventually agglomerated either during transit from the spark generator to the filtration step on the PTFE membrane or during the annealing.[24]

For comparison purposes, the surface of another polymer membrane was activated by a conventional wet two-step process (Figure 1), which required Sn sensitization. The membrane was first sensitized by immersing it in an aqueous solution containing $SnCl_2$ (8 mg), HCl (0.05 mL), and deionized (DI) water (49.95 mL), followed by rinsing with DI water. The activated membrane was accelerated by immersing it in an aqueous solution containing NaOH (1 g) and DI water (50 mL) to remove Sn species over the catalytic Pd particles, followed by rinsing with DI water. The subsequent activation was carried out in a $PdCl_2$ solution of $PdCl_2$ (4 mg), HCl (0.05 mL), and DI water (49.95 mL), followed by rinsing again with DI water. The ELD condition was as follows: $PdCl_2$, 1 g L^{-1}; $NH_3 \cdot H_2O$ (28%), 120 mL L^{-1}; HCl, 2 mL L^{-1}; NH_4Cl, 20 g L^{-1}; NaH_2PO_2, 10 g L^{-1}; temperature, 45 °C; pH, ~10; time, 10−40 min.

The electrochemical measurements (also in Figure 1) were performed using a VERSASTAT3-200 (Princeton Applied Research, Inc.) electrochemical analyzer and a conventional three-electrode electrochemical cell at 30 ± 0.4 °C. A Pt plate was used as the counter electrode. A saturated calomel electrode was used as the reference electrode. The working electrode was a rotating glassy carbon electrode (5 mm diameter) that was covered with part of the fabricated catalyst after being polished and cleaned by sonication. The current density in the electrochemical measurements was normalized to the geometrical surface area of the working electrode. The solution for the measurement was 5 M HCOOH.

Catalytic conversion (also in Figure 1) of toluene was carried out in a quartz fixed-bed reactor (37 mm inner diameter) at atmospheric pressure and temperatures between 100 and 300 °C. Toluene (air-balanced) was acquired from a compressed gas cylinder and a flow rate of the gas stream was controlled by a mass flow controller (MKS Instrument). An inlet concentration of 1000 ppm for toluene in a flow of 15 cm^3 h^{-1} was used, resulting in a space time of 16 000 $m_{gas}{}^3$ h^{-1} $m_{catalyst}{}^{-3}$. To avoid condensation of the reactant or any reaction product, all of the lines were heated above 100 °C. The concentrations of the toluene in the outlet gas stream were measured by a photoionization detection gas analyzer (Sniffer II, Kinsco, Inc.; lower detection limit of 0.01 ppm), which monitored the total VOC (TVOC). The steady-state conversion was obtained from the inlet (C_{inlet}^{VOC}) and outlet (C_{outlet}^{VOC}) concentrations of TVOC.

$$\text{conversion} = \frac{C_{inlet}^{VOC} - C_{outlet}^{VOC}}{C_{inlet}^{VOC}} \quad (1)$$

To avoid condensation in the tube system due to cooling by ambient air, we used a thermostatically heated tube system set to a preselected temperature of 300 °C. The absence of artifact from condensation was verified using a condensation particle counter (3025, TSI).

All experiments and measurements were performed four times and the following data described with averaged values.

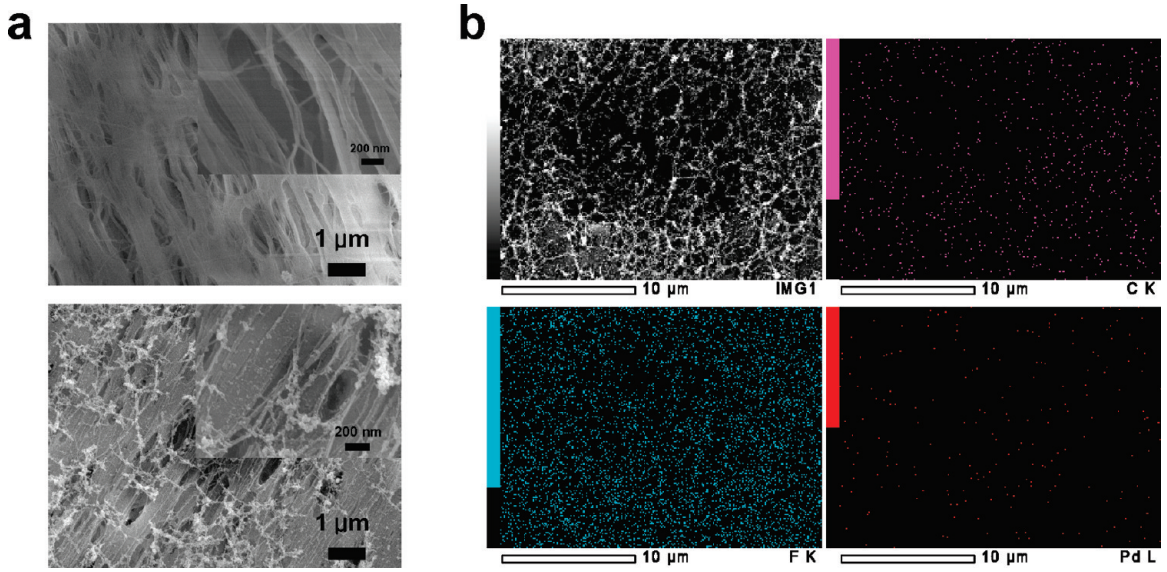

Figure 2. (a) SEM images of the pristine and activated surfaces of polymer membranes. (b) EDX results of the activated membrane.

RESULTS AND DISCUSSION

Size, Surface Density of a Pd Aerosol Seed, and Activation Intensity. The scanning electron microscopy (SEM; JSM-6500F, JEOL) images (Figure 2a) showed that the pristine membrane had a clean surface, while a number of particles were present on the activated membranes. The mean mode diameter of the single (or primary) nano seeds was approximately 4 nm, which had been proven by transmission electron microscopy in the earlier report.[24] From energy-dispersive X-ray (EDX; JED-2300, JEOL) spectroscopic analyses (Figure 2b), it was found that the pristine membrane contained C (31.8% of the number of atoms) and F (68.2% of the number of atoms), which might have originated from the membrane, while activated membranes contained a small amount of Pd (0.37−3.40% of the number of atoms). The first image of the bottom of the membrane in Figure 2b shows a different scaled micrograph of the activated membrane for 1.77% Pd of the number of atoms. The following three images show the EDX maps of the dotted area in the first image. These maps corresponded to C, F, and Pd, respectively. The dots in these images indicated the positions of each element in the first image. However, the dots in the Pd map were not well corresponded (not dense) because the Pd detection led to an apparent homogeneous surface density of Pd nano seeds, including the seeds located in the membrane. From the above characterizations, the activation intensity $[I_a(D_p)]$ of the substrate is defined as follows:[25]

$$I_a(D_p) = Qt_a A_m^{-1} m^{-1} \int_0^\infty \eta(D_p)\, C_a(D_p)\, dD_p \qquad (2)$$

where Q is the flow rate of the carrier gas, t_a is the activation time, A_m is the surface area of the membrane, m is the mass of the membrane, and $C_a(D_p)$ is the surface density of the Pd nano seed. The activation intensity was selected to be approximately 0.43−3.44 cm^2 of Pd nano seed m^{-2} of membrane (or 3.49−27.90 μg of Pd m^{-2} of membrane).

Growth Kinetics and Trend of Pd−P Film Formation. The SEM images in Figure 3a show the trend of film formation on the activated surface of the membrane with the ELD time ranging from 10 to 40 min for activations of 0.43−3.44 cm^2 of Pd nano seed m^{-2} of membrane. The deposited film showed a gray color. In Figure 3a, the particles (~210 nm) formed initially (10 min of ELD) on the top of the Pd nano seeds. The particles had a random orientation, resulting in an irregular disposition. Because the Pd nano seeds were located at different areas of the membrane surface, the probability of film formation on different seeds during ELD was expected to be different, i.e., a shadowing effect. Because of an initial microstructural nonuniformity, some nuclei could grow faster than others, leading to nonuniformity of the formed film microstructure. The number of particles increased progressively with increasing ELD time, through three-dimensional growth of laterally coalescent hemispherical particles, which was similar to observations reported by Robertis et al.,[16] leading to a more compact filming, which covered most of the membrane surface. Moreover, with higher activation intensities, continuous granular films were formed faster, more rapidly covering the membrane surface. Thus, both separate particles and film can also be achieved by adjusting the activation intensity. Nevertheless, the observed voids were likely due to the trapping of hydrogen gas, which was formed by the combination of hydrogen radical species produced during the first steps of the hypophosphite oxidation (also refer to eq 4).[26] Because of the known capacity of Pd for hydrogen adsorption and/or absorption, completely dense films were hardly obtained. In addition, from the standard tape test using 3M 2503710, it is confirmed that there was a smaller decrease of Pd−P (14% mass) with annealing (at 240 °C) after activation than without the annealing case (67% mass).

Comparison of the Pd−P Film Roughness between Pd Aerosol and Sn−Pd Activations. Figure 3b shows flattened atomic force microscopy (AFM; Nanoscope IIIa, Advanced Surface Microscopy, Inc.) images of the film topograph (11.72 cm^2 of Pd nano seed m^{-2} of membrane activation intensity) obtained in the tapping mode. After 10 min of ELD, the film presented a rough morphology, due to a large number of almost spherical clusters. By an increase of the ELD time (40 min), cluster coalescence could occur and less rough and more uniform morphology was observed. The thickness and arithmetic mean

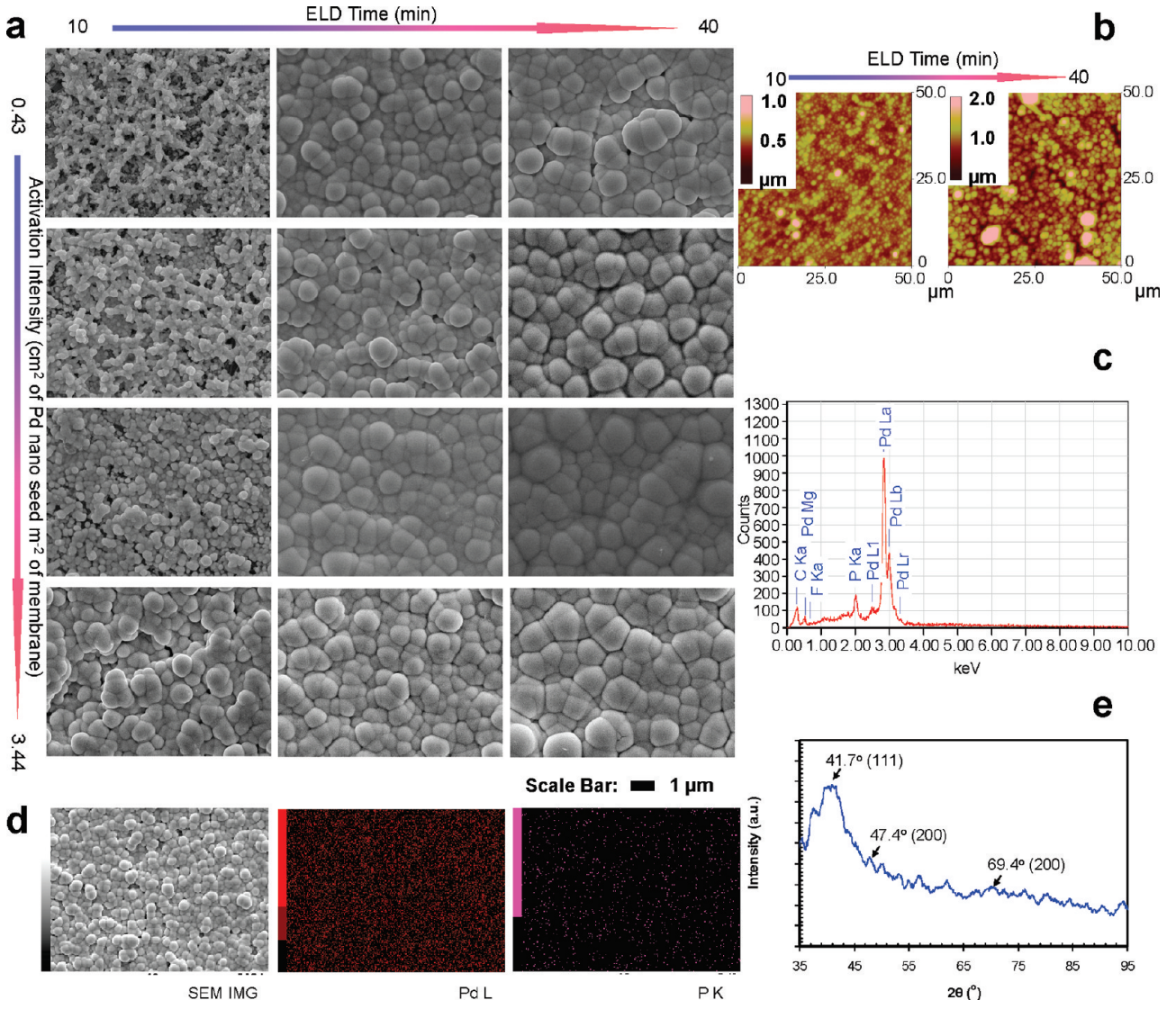

Figure 3. (a) SEM images of electroless films (10, 20, and 40 min ELD) for different activation intensities. (b) Topographs of electroless deposits of 10 and 40 min ELDs for 1.72 cm^2 of Pd nano seed m^{-2} of membrane activation intensity. (c) EDX profile of the catalyst (40 min of ELD) for 1.72 cm^2 of Pd nano seed m^{-2} of membrane activation intensity. (d) XRD result of the catalyst (40 min of ELD) for 1.72 cm^2 of Pd nano seed m^{-2} of membrane activation intensity.

roughness of the 10−40 min depositions were approximately 0.8−1.4 μm and 59.5−153.3 nm, respectively. The estimated dimensional growth rates of 0.43−3.44 cm^2 of Pd nano seed m^{-2} of membrane activation intensities were 27.5−45.0 nm min^{-1} for the case of a 40 min deposition.

Elemental Analysis and Film Formation Mechanism. The Pd Lα peaks (Figure 3c) for 40 min of deposition (1.72 cm^2 of Pd nano seed m^{-2} of membrane) were detected for the film, confirming the formation of Pd films by the ELD. Noticeably, a small peak corresponding to P Kα also appeared for all of the samples, indicating the inclusion of P in Pd (i.e., the formation of a Pd−P alloy instead of pure Pd). Correspondingly, the dot maps (Figure 3d) also show a homogeneous element (Pd and P) distribution. The inclusion of a P atom in the Pd matrix could be ascribed to the codeposition of Pd (denoted as Pd↓ in eq 3) and P (denoted as P↓ in eq 4) elements in the ELD bath. Generally, the bath containing Pd ions (Pd^{2+}) from $PdCl_2$ and hypophosphite ions ($H_2PO_2^-$) from NaH_2PO_2 might be introduced to the Pd−P film via the following reactions:[27]

$$Pd^{2+} + H_2PO_2^- + H_2O = Pd\downarrow + H_2PO_3^- + 2H^+ \quad (3)$$

$$2H_2PO_2^- + H^\bullet = P\downarrow + H_2PO_3^- + \frac{1}{2}H_2\uparrow + H_2O \quad (4)$$

The results indicated that the P atom coexisted with the Pd film and the atomic ratios of P to Pd (the degree of amorphicity)[28] were in the range of 7.64 ($Pd_{92.9}P_{7.1}$)−7.89 ($Pd_{92.7}P_{7.3}$) for 0.43−3.44 cm^2 of Pd nano seed m^{-2} of membrane activation intensities for the 40 min ELD. It was found in the experiments that the activation intensity had little effect on the chemical deposition of the Pd−P films. The Pd−P film amounts were also obtained from inductively coupled plasma atomic emission spectroscopy (ICPAES; Elan 6000, Perkin-Elmer) analyses.

dx.doi.org/10.1021/am200613w |ACS Appl. Mater. Interfaces 2011, 3, 2912–2918

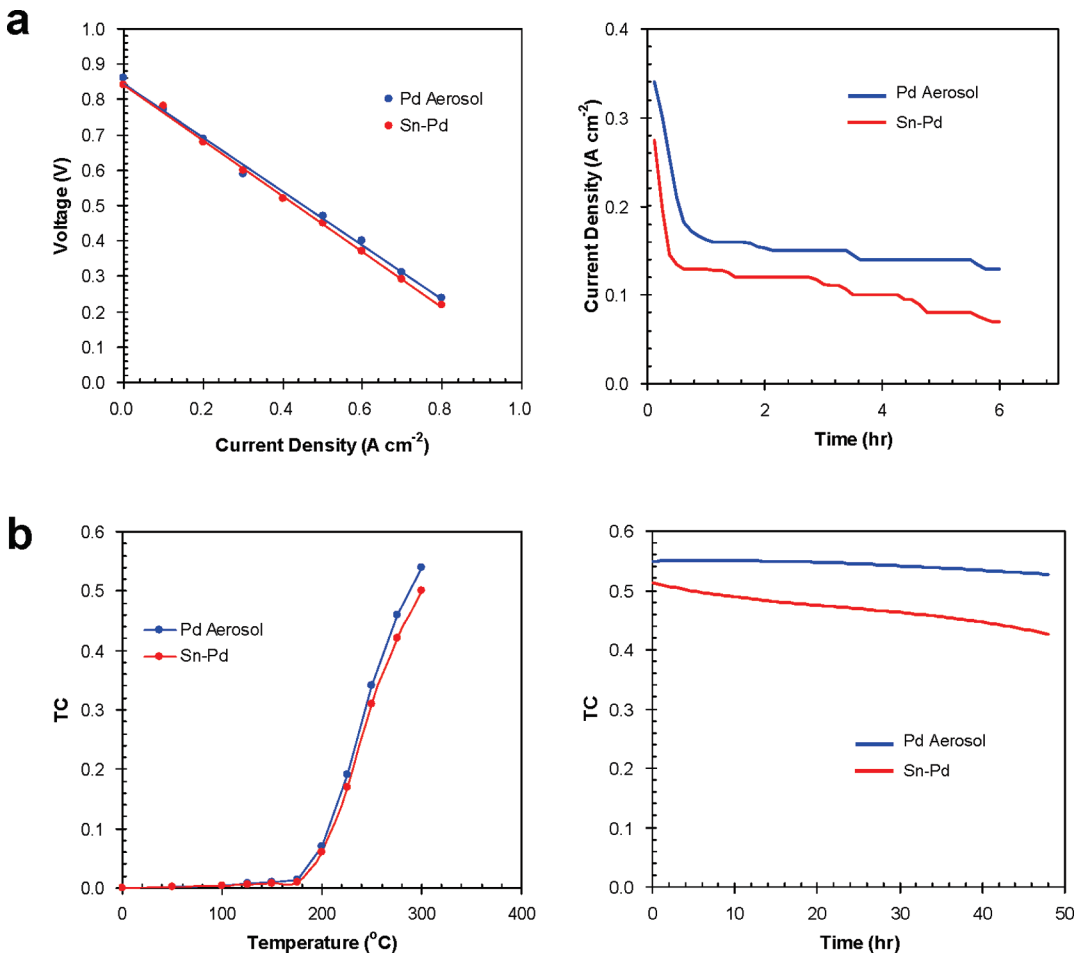

Figure 4. (a) Polarization plots with FAO (left) and time dependences of the current density at a voltage of 0.53 V at 30 °C. (b) TC with different temperatures (left) and the TC stability with operation times (right).

Analyses for the Pd and P elements were performed as follows. A weighed portion of the sample (about 0.01 g) was dissolved in 2 mL of boiling HNO_3. The resulting solution was diluted with water to 50 mL in a volumetric flask. The P content was determined photocolorimetrically by the standard procedure.[29] The deposition rates (for 40 min ELD) for 0.43−3.44 cm^2 of Pd nano seed m^{-2} of membrane activation intensities were 13.1−28.3 μg of Pd−P film cm^{-2} min^{-1}, respectively.

X-ray Diffraction of the Pd−P Film. Diffraction peaks at 40.6, 46.4, and 68.2° corresponded to the (111), (200), and (220) crystal faces of Pd,[14] respectively; however, the diffraction peaks (at 41.7, 47.4, and 69.4°) of the fabricated film (for the 40 min ELD with 1.72 cm^2 of Pd nano seed m^{-2} of membrane activation intensity) (Figure 3d) were much broader than those of the Pd film, showing that the relative crystallinity of the fabricated film was much lower than that of the Pd film. The lattice parameters a_{fcc} for the Pd film with a face-centered cubic (fcc) structure were evaluated from the angular position of the Pd(220) peak maximum according to the following formula:[30]

$$a_{fcc} = \frac{\sqrt{2}\lambda_{K\alpha_1}}{\sin \theta_{max}} \quad (5)$$

where $\lambda_{K\alpha_1}$ is 0.154 056 nm. The calculated lattice parameters were 0.3903 nm for the Pd−P film (cf. 0.3913 nm for the Pd film in a previous report).[14] This indicated that the crystal lattice of Pd contracted in the presence of P. Therefore, P had entered into the crystal lattice of Pd at the atomic level.[31]

Catalytic Activities and Stability of Pd−P Films. There was no significant difference in the polarization between the Pd aerosol and Sn−Pd activations, as shown in Figure 4a (left). Time dependence changes in the current densities (the short-term durability test) of the catalyst with both activations were observed at a constant voltage of 0.53 V, as is also shown in Figure 4a (right). The current density significantly dropped in 6 h of operation of the catalysts with both activations. However, the current drop with the Sn−Pd activation was more than that with the Pd aerosol activation. The above electrochemical results demonstrated that when the Pd−P film was fabricated from the aerosol activation, the electrocatalytic performance of the catalyst for the oxidation of formic acid was improved. In particular, the electrocatalytic stability of formic acid oxidation for the aerosol activation was much better than that from the Sn−Pd activation. It was possible that the performance loss of the catalyst from the Sn−Pd activation was caused by higher resistance and a substantially lower oxidation reaction rate. Indeed, when the Sn−Pd activation was performed, impurities such as Sn (1.44% of the number of atoms; electrical resistivity, 11.5 $\mu\Omega$ cm > 10.5 $\mu\Omega$ cm for Pd) and Cl (1.82% of the number of atoms; electrical resistivity, $>10^9$ $\mu\Omega$ cm) compounds, resulting in an increase

in the resistance from 0.14 (aerosol activation) to 0.26 Ω cm^2 (Sn−Pd activation). Moreover, according to a report,[32] the crystal sizes of the Sn−Pd seed were very small (ranging from subnanometers to a few nanometers). These sizes could be easily oxidized (i.e., increase in the resistance) during the oxidation reaction, and thus a further decrease in the catalytic activity of the composite catalyst might also be induced. In addition, a comparison between the Pd−P and Pd films from aerosol activation was also evaluated, and the time dependence electrocatalytic activity of the Pd film only reached 0.81 in comparison with the Pd−P film. From X-ray photoelectron spectroscopy (AXIS HIS, Kratos) analyses, for the Pd film,[14] the Pd $3d_{3/2}$ peak at 340.6 eV and the Pd $3d_{5/2}$ peak at 335.4 eV were assigned to Pd^0, while the Pd $3d_{3/2}$ and Pd $3d_{5/2}$ peaks of Pd^0 for the Pd−P film were at 341.0 and 335.9 eV, respectively. The Pd^0 peaks for the Pd−P film were 0.4 eV more positive than those of the Pd film. This is due to the fact that when Pd interacted with P, Pd would donate electrons to P, causing a decrease in the 3d electron density of Pd. Pd with low 3d electron density did not easily bind to the COOH intermediate, and then the surface $(COOH)_{ads}$ coverage was reduced. Thus, formic acid could be easily oxidized through a direct pathway.[33]

The steady-state conversion of toluene as a function of the reaction temperature is shown in Figure 4b (left). The steady-state conversion increased with the reaction temperature, and the trend was similar to that in a report by Bedia et al.[7] The maximum reaction temperature was chosen to be 300 °C to prevent the burnoff of the polymer membrane. Thus, the conversion efficiencies were low compared to those of other classical pollution abatement methods. The Pd−P film for the Pd aerosol activation was more stable for 48 h than that from the Sn−Pd activation (Figure 4b) (right), with no significant changes in the conversion during the extent of the experiment. Differences in the conversion stability (i.e., deactivation) were found that probably resulted from the difference between the activations. The Sn and Cl compounds in the film from the Sn−Pd activation might affect the deterioration by unwanted blocking, residing, or alloying from the compounds. Owing to a very small size,[32] the Sn−Pd seeds (also containing Cl) could be easily merged with the Pd−P film at the reaction temperature as a molten form,[19] and thus the deterioration might be induced. In addition, a comparison between the Pd−P and Pd films from aerosol activation was also evaluated, and the steady-state conversion of the Pd film was only reached at 0.69 in comparison with the Pd−P film. Previous reports[34,35] stated that Pd with the low 3d electron density (for the Pd−P film) was more active than metallic Pd (for the Pd film) for the catalytic oxidation reaction. During the oxidation, moreover, Pd might be easily oxidized by CO_2 and H_2O,[6,7] but after P was added to the Pd matrix, Pd might be not be easily oxidized because P was already a nonmetallic element. Products from the toluene conversion might be more hazardous than toluene especially with fluorine from the substrate, and further characterization of the products for real application would be recommended.

CONCLUDING REMARKS

The composite catalysts of the Pd−P film on the PTFE membrane were fabricated by the novel ELD, and its catalytic activities of FAO and TC were performed. The novel ELD brought an interesting two-step deposition process, leading to controlled roughness of the Pd−P film on the PTFE membrane by surface activation with deposition of Pd aerosol nanoparticles produced by a spark discharge, followed by electroless bath immersion. The prepared samples from the aerosol activation had more stable FAO and TC activities than those from the conventional Sn−Pd activation, and their better stabilities could be attributed to their purity from the aerosol activation that only introduced pure Pd. This strategy may be attractive for various scientific and/or engineering applications for catalytic electrodes, catalysts, etc., because the aerosol activation of the support is simple, environmentally friendly, and effective (with fewer impurities).

A further study focuses on activities (conversion of reactants) and selectivities (of target products) together with elucidation of the structural features of catalysts, and their relationship to the catalytic performance and mechanistic details of the catalytic reaction is now in preparation to publish elsewhere.

AUTHOR INFORMATION

Corresponding Author

*Tel.: +82 41 540 5819. Fax: +82 41 540 5818. E-mail: ywkim@hoseo.edu.

REFERENCES

(1) Ha, S.; Adams, B.; Masel, R. I. *J. Power Sources* **2004**, *128*, 119.
(2) Zhu, Y. M.; Zakia, K.; Masel, R. I. *J. Power Sources* **2005**, *139*, 15.
(3) Persson, K.; Ersson, A.; Jansson, K.; Iverlund, N.; Jaras, S. *J. Catal.* **2005**, *231*, 139.
(4) Thomas, F. S.; Masel, R. I. *Surf. Sci.* **2004**, *573*, 169.
(5) Baldauf, M.; Kolb, D. M. *J. Phys. Chem.* **1996**, *100*, 11375.
(6) Zhang, L.; Tang, Y.; Bao, J.; Lu, T.; Li, C. *J. Power Sources* **2006**, *162*, 177.
(7) Bedia, J.; Rosas, J. M.; Rodríguez-Mirasol, J.; Cordero, T. *Appl. Catal., B* **2010**, *94*, 8.
(8) Bhuvana, T.; Kumar, G. V. P.; Kulkarni, G. U.; Narayana, C. *J. Phys. Chem. C* **2007**, *111*, 6700.
(9) Zabetakis, D.; Dressick, W. J. *ACS Appl. Mater. Interfaces* **2009**, *1*, 4.
(10) Kuo, L.-C.; Huang, Y.-C.; Lee, C.-L.; Yen, Y.-W. *Electrochim. Acta* **2006**, *52*, 353.
(11) Yang, L.; Bai, S.; Zhu, D.; Yang, Z.; Zhang, M.; Zhang, Z.; Chen, E.; Cao, W. *J. Phys. Chem. C* **2007**, *111*, 431.
(12) Demirel, M. C.; Cetinkaya, M.; Singh, A.; Dressick, W. J. *Adv. Mater.* **2007**, *19*, 4495.
(13) Huang, Y.; Dittmeyer, R. *J. Membr. Sci.* **2007**, *302*, 160.
(14) Byeon, J. H.; Hwang, J. *ACS Appl. Mater. Interfaces* **2009**, *1*, 261.
(15) Podestá, J. J.; Piatti, R. C. V. *Int. J. Hydrogen Energy* **1997**, *22*, 753.
(16) Robertis, E. D.; Neves, R. S.; Abrantes, L. M.; Motheo, A. J. *J. Electroanal. Chem.* **2005**, *581*, 86.
(17) Cristina, M.; Oliveira, F. *Electrochim. Acta* **2008**, *53*, 8138.
(18) Byeon, J. H.; Park, J. H.; Hwang, J. *J. Aerosol Sci.* **2008**, *39*, 888.
(19) Byeon, J. H.; Kim, J.-W. *Langmuir* **2010**, *26*, 11928.
(20) Borra, J. P. *Plasma Phys. Controlled Fusion* **2008**, *50*, 124036.
(21) Bau, S.; Witschger, O.; Gensdarmes, F.; Thomas, D.; Borra, J.-P. *J. Nanopart. Res.* **2010**, *12*, 1989.
(22) Liu, Y.-L.; Yu, C.-H.; Lai, J.-Y. *J. Membr. Sci.* **2008**, *315*, 106.
(23) Wu, J. C. S.; Chang, T. Y. *Catal. Today* **1998**, *44*, 111.
(24) Borra, J.-P. *J. Phys. D: Appl. Phys.* **2006**, *39*, R19.
(25) Byeon, J. H.; Ko, B. J.; Hwang, J. *J. Phys. Chem. C* **2008**, *112*, 3627.
(26) Robertis, E. D.; Abrantes, L. M.; Motheo, A. J. *Thin Solid Films* **2008**, *516*, 6266.
(27) Chu, S.-Z.; Kawamura, H.; Mori, M. *Electrochim. Acta* **2007**, *53*, 92.

(28) Robertis, E. D.; Fundo, A. M.; Motheo, A. J.; Abrantes, L. M. *J. Braz. Chem. Soc.* **2005**, *16*, 103.
(29) Belykh, L. B.; Skripov, N. I.; Belonogova, L. N.; Umanets, V. A.; Shmidt, F. K. *Russ. J. Appl. Chem.* **2007**, *80*, 1523.
(30) Radmilovic, V.; Gasteiger, H. A.; Ross, P. N. *J. Catal.* **1995**, *154*, 98.
(31) Cheng, L.; Zhang, Z.; Niu, W.; Xu, G.; Zhu, L. *J. Power Sources* **2008**, *182*, 91.
(32) Byeon, J. H.; Hwang, J. *Surf. Coat. Technol.* **2008**, *203*, 357.
(33) Stojewski, M.; Kowalska, J.; Jurczakowski, R. *J. Phys. Chem. C* **2009**, *113*, 3707.
(34) Yazawa, Y.; Yoshida, H.; Takagi, N.; Komai, S.-i.; Satsuma, A.; Hattori, T. *Appl. Catal., B* **1998**, *19*, 261.
(35) Burch, R.; Loader, P. K.; Urbano, F. J. *Catal. Today* **1996**, *27*, 243.